Available online at BCREC website: https://bcrec.id

Bulletin of Chemical Reaction Engineering & Catalysis, 18 (4) 2023, 615-626

Research Article

Kinetic Study of the Aluminum–Water Reaction Using NaOH/$NaAlO_2$ Catalyst for Hydrogen Production from Aluminum Cans Waste

Nur Fadhilah[1], Maktum Muharja[2,*], Doty Dewi Risanti[1,*], Ruri Agung Wahyuono[1], Dendy Satrio[3], Achri Isnan Khamil[2], Siska Nuri Fadilah[4]

[1]Department of Engineering Physics, Institut Teknologi Sepuluh Nopember, Kampus ITS Sukolilo, Surabaya 60111, East Java, Indonesia.
[2]Department of Chemical Engineering, Universitas Jember, Jl. Kalimantan No. 37, Jember 68121, East Java, Indonesia.
[3]Department of Ocean Engineering, Institut Teknologi Sepuluh Nopember, Surabaya, 60111, Indonesia.
[4]Environmental Management Postgraduate Program, Universitas Sriwijaya, Jl. Padang Selasa No. 524, Palembang 30131, South Sumatra, Indonesia.

Received: 21st September 2023; Revised: 27th October 2023; Accepted: 28th October 2023
Available online: 31st October 2023; Published regularly: December 2023

Abstract

The presence of oxide layers covering the surface of aluminum is known to impede the hydrogen production reaction. These oxide layers can be broken by adding catalysts and increasing the aluminum-water reaction temperature. Common catalysts used are alkaline catalysts that are capable of achieving high hydrogen production rates in a short time at lower temperatures, while intermediate temperatures of above 50 °C can accelerate the hydration reaction of the oxide layer. Herein, the mixture of NaOH and $NaAlO_2$ catalysts was employed to attain a stable $NaAlO_2$ solution and continuous reaction of NaOH and aluminum. This research analyzes the influence of temperature between 32 and 80 °C on the aluminum, 0.3 M NaOH and 0.001 M $NaAlO_2$ catalysts solution at atmospheric pressure. All solutions produces a similar hydrogen yields and rate. Solutions containing $NaAlO_2$ indicate reverse reaction that surpressing the $Al(OH)_3$ precipitation. Residue from the reaction is investigated using X-ray Diffraction (XRD), Fourier Transform Infra Red (FTIR), and Scanning Electron Microscope (SEM). The volume of hydrogen produced is evaluated using a mathematical mass reduction and shrinking core model. The rate of hydrogen production depends largely on the aqueous solution's temperature, with an activation energy of 47.4 kJ/mol. Based on the findings, it is readily apparent that the reaction only produced gibbsite and bayerite, with gibbsite and bayerite being dominant at 32–70 °C and 80 °C, respectively. The mass reduction model fits well with the present results with only an average 5.1 ml deviation, whereas the shrinking core model generally tends to result in underestimated values with an average deviation of 23.9 ml.

Copyright © 2023 by Authors, Published by BCREC Group. This is an open access article under the CC BY-SA License (https://creativecommons.org/licenses/by-sa/4.0).

Keywords: Aluminum waste; Hydrogen; Modeling; Oxide Layers

How to Cite: M. Muharja, N. Fadhilah, D.D. Risanti, R.A. Wahyuono, D. Satrio, A.I. Khamil, S.N. Fadilah (2023). Kinetic Study of the Aluminum–Water Reaction Using NaOH/$NaAlO_2$ Catalyst for Hydrogen Production from Aluminum Cans Waste. *Bulletin of Chemical Reaction Engineering & Catalysis*, 18(4), 615-626 (doi: 10.9767/bcrec.20041)

Permalink/DOI: https://doi.org/10.9767/bcrec.20041

1. Introduction

The increasing demand for energy for human needs, the depletion of fossil fuels, and growing environmental awareness have led most researchers to seek new and renewable energy sources [1–3]. The Energy Information Administration (EIA) predicts that global energy demand will increase by 25% by 2050, driven by population and economic growth, while the

* Corresponding Author.
Email: maktum@unej.ac.id (M. Muharja);
risanti@ep.its.ac.id (D.D. Risanti)

share of renewable energy is expected to grow from 14% in 2015 to 22% by 2060 [4]. Therefore, to balance the pace of renewable energy consumption and mitigate negative environmental impacts, a transition and diversification of energy sources toward sustainable renewable power generation is required. One prominent area of renewable energy development currently being pursued by researchers is the production of hydrogen as an energy carrier and fuel source [5–8].

Hydrogen is classified as a renewable and clean energy source because its combustion process does not produce pollutants like CO and CO_2 gases [9,10]. There are various methods for producing hydrogen, including coal gasification [11-13], water electrolysis [14-17], natural gas steam reforming [18-20], water splitting [24-26], and hydride chemical reactions [27]. However, each of these methods has its drawbacks, such as high cost, low efficiency, environmental pollution, and the need for external energy sources derived from fossil fuels. The hydrolysis reaction between metal and water is one of the most promising ways to produce clean and cost-effective hydrogen. This method has been extensively studied over the past few decades. Some of the metals studied for hydrogen generation performance include aluminum [28], magnesium [29], and zinc [30]. In recent years, aluminum–based renewable energy technology has been massively researched as a high-energy-density alternative hydrogen source [31]. Aluminum waste is abundantly available, making it a more environmentally friendly method [32]. The energy in aluminum can be released through a reaction with water to produce heat and hydrogen. Therefore, aluminum has the potential to be a more efficient hydrogen producer compared to other metals.

At room temperature, hydrogen production from the aluminum–water reaction is hindered due to the presence of an aluminum oxide (Al_2O_3) layer on the surface of aluminum, which prevents direct contact between water and aluminum. This phenomenon is known as passivation [31]. Several methods have been employed to address this issue, including the addition of $NaAlO_2$ to inhibit the formation of the Al_2O_3 layer and the introduction of alkali promoters / catalysts [33], hydroxide materials [28], as well as alloys or dopants [3] during the hydrolysis process. The addition of catalysts serves not only to eliminate the Al_2O_3 layer but also to lower the activation energy and accelerate the reaction. Commonly used catalysts in the aluminum–water reaction are hydroxide catalysts like NaOH and KOH, with NaOH being more suitable due to its cost-effectiveness while yielding similar hydrogen results [28]. The mixture of NaOH and $NaAlO_2$ has been known to be applied for the surface treatment of aluminum and its alloys, particularly for plasma electrolytic oxidation. The process depends on the stability of the alkaline solution by which the addition of NaOH in $NaAlO_2$ solution can lead to a stable solution, *i.e.* retention of aluminate ions ($Al(OH)_4^-$) to decompose into $Al(OH)_3$ [34]. Generally, the aluminum in an alkaline solution reacts as follows [35]:

$$2Al + 6H_2O + 2NaOH \rightarrow 2NaAl(OH)_4 + 3H_2 \quad (1)$$

$$NaAl(OH)_4 \rightarrow NaOH + Al(OH)_3 \quad (2)$$

The first reaction indicates that as the hydrogen is released, a hydrated sodium aluminate is formed. This hydrated sodium aluminate is then decomposed into NaOH and $Al(OH)_3$ when the aluminate concentration exceeds its saturation limit as seen in the second reaction [36]. The main challenge in controlling the production of hydrogen lies in the understanding of the second reaction as the equilibrium is not exclusive. The primary goal of this research is not to improve the precipitation of $Al(OH)_3$, but to NaOH regeneration by facilitating a sufficient amount of aluminate leading to further decomposition. Since hydrogen is generated through the first reaction, controlling the second reaction is important.

The equilibrium's constant changes as a result of a temperature rise, which causes an increase in the equilibrium concentration of $NaAl(OH)_4$. This rise in $NaAl(OH)_4$ equilibrium concentration creates a greater NaOH equilibrium concentration. As a result, the sodium hydroxide concentration is substantially higher, leading to an increased hydrogen flow rate. According to Le-Chatelier's principle [37], when an equilibrium reaction's conditions are changed, the position of equilibrium shifts to counteract the change to reestablish the equilibrium. Applying this principle to reaction (2), if NaOH is removed, the equilibrium shifts to the right of the reaction. Then, higher quantities of NaOH are produced while the amount of $Al(OH)_3$ produced is reduced.

The effect of catalysts on reaction kinetics can be approximated through mathematical modeling. Atmospheric methods can be modeled either as a shrinking core or through a mass reduction model [38]. The shrinking core model examines the entire aluminum hydra-

Copyright © 2023, ISSN 1978-2993

tion process, including the formation of hydroxide products based on reaction stages. On the other hand, the mass reduction method, as proposed by Berna *et al*. [39], focuses on the active surface and is related to the rate of thickness reduction over time. Studies on the kinetics and mechanisms of hydrogen production from the aluminum–water reaction have been conducted [32]. However, there has been no intensive modeling of the kinetics of hydrogen production from aluminum–water using hydroxide promoters under atmospheric conditions. The influence of temperature and catalysts on hydrogen yield is also discussed. Reaction kinetics are analyzed to determine the effect of temperature on the reaction, approximated through shrinking core and mass reduction modeling.

2. Materials and Methods

2.1 Materials

The aluminum used is in the form of beverage can waste aluminum with a thickness of 0.65 mm. Sodium hydroxide (NaOH), sodium aluminate ($NaAlO_2$), and distilled water were purchased from PT Sumber Ilmiah Persada, Surabaya, Indonesia.

2.2 Pretreatment of Beverage Cans Aluminum

The can's lid and bottom part were removed because they were made from different aluminum alloys. The outer surface of the can was cleaned to remove the protective paint and polymer coating that covered both the outside and inside of the can through polishing using SiC abrasive paper of 400 grit. The major polymeric coating used in cans is epoxy resin to prevent the soda from reacting with aluminum. This cleaning procedure is undertaken until the painted surface is removed completely. The aluminum can is subsequently cut into pieces having dimensions of 2×3 cm^2.

2.3 Aluminum–Water Reaction

In the atmospheric reactor experiment, 0.2 g of aluminum waste is reacted with a mixture of 0.3 M NaOH and 0.01 M $NaAlO_2$ solution in a four-necked flask. The reaction is conducted at varying temperatures of 32, 40, 50, 60, 70, and 80 °C, with observations made every 10 min. The atmospheric reactor used for the aluminum–water reaction consists of a four-necked flask connected to an inverted burette to measure the volume of hydrogen produced. The change in water level in the inverted burette was used to calculate the amount of H_2 gas produced and measurements were repeated three times for each condition, resulting in a relative standard deviation of about 3%. From the obtained H_2 production curve, one can estimate the maximum flow rate from its maximum slope and its respective standard deviation was 0.18 $cm^3.min^{-1}$. The concentration and temperature of the generated hydrogen reaction are measured using an MQ-8 sensor and thermocouple connected to an Arduino, which is linked to a computer for data reading (see Figure 1).

The percent yield of hydrogen was estimated by using the following equation [6]:

$$\%Yield = \frac{Actual\ H_2\ yield}{Theoretical\ H_2\ yield} \times 100\% \quad (3)$$

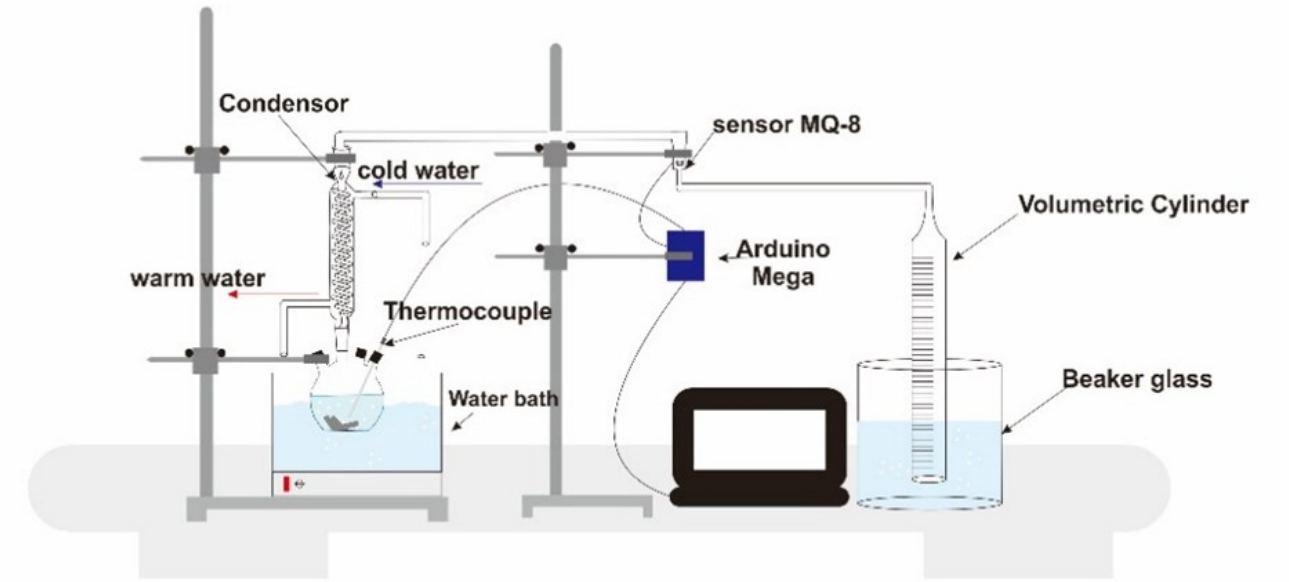

Figure 1. Instrumentation scheme for an atmospheric reactor.

Copyright © 2023, ISSN 1978-2993

The following equations were used to determine the theoretical hydrogen yield [28]:

$$PV_{H_2} = n_{H_2}RT \quad (4)$$

$$H_2\ mol\left(n_{H_2}\right) = \frac{Al\ experimental\ mass}{Al\ molar\ mass} \times 1.5 mols \times H_2\ molar\ mass \quad (5)$$

where, P is the pressure (1 atm), R is the gas constant 0.0821 L.atm/(mol.K); T is the operating temperature (K); n is the molar of hydrogen, and V is the theoretical hydrogen yield.

2.4 Characterizations

X-Ray Fluorescence (XRF) analysis (Thermo Scientific NitonTM XL3T) was conducted on the aluminum waste cans before the reaction to determine the elemental composition of the aluminum waste. The results of the aluminum waste can composition are presented in Table 1, which closely approximates the aluminum series AA3105. Final characterization after the reaction included X-Ray Diffraction (XRD), Fourier-Transform Infrared Spectroscopy (FTIR), and Scanning Electron Microscopy with Energy Dispersive X-Ray Spectroscopy (SEM-EDX). XRD testing (Phillips X'pert MPD) was performed to ascertain the crystal structure of the reaction products. FTIR (Thermo Nicolet i510) was employed to identify the functional groups present in the final residue of the aluminum waste at a wavenumber ranging from 500 to 4000 cm^{-1}. pH was measured by using pH meter Mettler Toledo S220.

2.5 Mathematical Model and Data Analysis

The measured volume data at each temperature variation is compared using mathematical modeling. The thickness of the aluminum can waste in the slab-shaped aluminum modeling is utilized to predict the reaction time from the start of the reaction until total completion, considering the smallest side since it will be consumed first, assuming that the rate of aluminum hydration on each side is the same. The mass reduction model (MRM) proposed by Berna *et al*. [39] and the shrinking core model (SCM) by Wang *et al*. [38] are employed.

The aluminum can waste is modeled as shown in Figure 2, where p is the thickness of the sheet, a is the width, and L is the length. The rate of aluminum being consumed depends on the thickness reduction e (mm/minutes) of all active surfaces as a function of time t. This model is valid up to the thickness p is all consumed. Hence, in the mass reduction model, the calculation of the active aluminum surface area is described in Equation (6):

$$S_{Al,t} = \frac{2W_{Al,0}\eta}{\rho_{Al}Lap}\left[\left(L'+a'+2e\right)*\left(p'+2e\right)+\left(L'*a'\right)\right] \quad (6)$$

where, e represents the aluminum reduction rate, $W_{Al,0}$ is the initial mass, r_{Al} is the aluminum density, and η is the aluminum purity percentage. The aluminum purity percentage is obtained from XRF data (Table 1). From the surface area value, the theoretical volume of hydrogen is calculated using Equation (7) [39].

$$V_{H_2} = \frac{3\rho_{Al}}{2M_{Al}}\frac{RT}{P}\sum_{t=0}^{n} S_{Al,t}e \quad (7)$$

Equation (8) represents the SCM equation in the form of a *slab*. The SCM is developed with a three-phase reaction approach, including thin film diffusion, chemical reaction, and ash control diffusion (Equations (9)–(11)).

$$Ra = -\frac{1}{b_2}\frac{dN_{B2}}{dt} = -\frac{dN_A}{dt} \quad (8)$$

$$Ra = 2apk_dC_{aw} \quad (9)$$

$$Ra = 2apk_{c2}C_{aw} \quad (10)$$

$$Ra = 2apD_e\frac{dCa}{dt} \quad (11)$$

Wang's mathematical model is modified for a slab geometry as follows:

$$V_{c2} = apL_{Grow} - apL_c \quad (12)$$

Table 1. The results of the XRF analysis of the aluminum can composition.

Element	Composition (%)
Al	93.4
Si	0.4
Mn	3.2
Fe	1.8
Cu	0.9
Zn	0.3

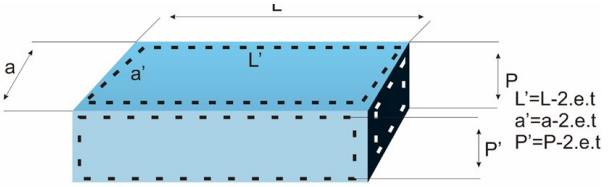

Figure 2. Mathematical modeling of aluminum reaction.

Copyright © 2023, ISSN 1978-2993

3. Results and Discussion

3.1 Hydrogen Production with NaOH+$NaAlO_2$ Catalyst

The influence of temperature on the volume and concentration of hydrogen is explained by the phenomenon that at higher operating temperatures, the reaction occurs faster, resulting in higher hydrogen yields (Figure 3). Hydrogen production increased from 0.13 mmol/gram to 0.54 mmol/gram at room temperature (32 °C to 80 °C) due to increased molecular movement and higher mass transfer rates. The volume of hydrogen produced also increased significantly from 160 mL to 240 mL. According to Kandasamy *et al.* [41], during hydrogen production, the aluminum concentration at the surface decreases as the formation of a diffusion-controlled layer on the surface progresses, leading to a continuous decrease in aluminum thickness as the temperature increases. This drives the dissolved species away from the reactive surface. Since it is controlled by diffusion, the increase in the reaction temperature improves the hydrogen generation rate and the hydrogen yield (Figure 4). The energy activation obtained from a temperature-dependent series via Arrhenius approximation for NaOH+$NaAlO_2$ solution is 47.4 kJ/mol. This value is still in the range obtained for NaOH only as reported by Zhuk *et al.* [42], for high-purity aluminum (greater than 99.9%), *i.e.*, of about 46-53 kJ.mol^{-1} in a temperature range

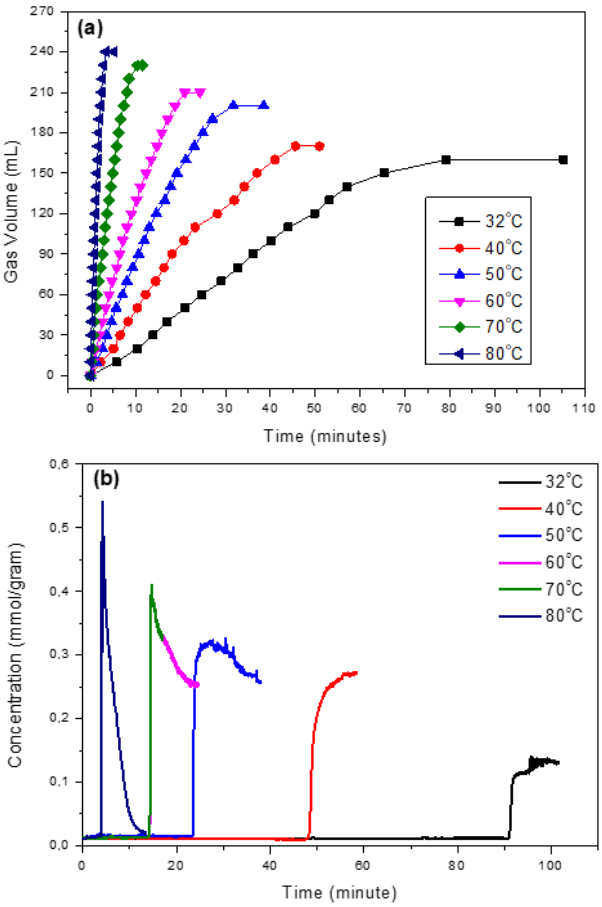

Figure 3. (a) Volume and (b) Concentration of hydrogen over time.

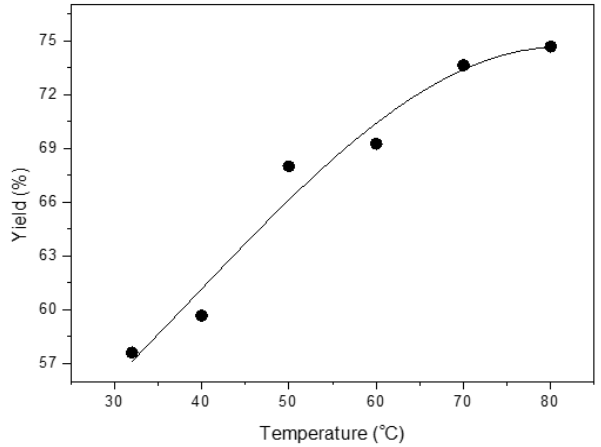

Figure 4. The hydrogen yield of NaOH and $NaAlO_2$ solution as a function of reaction temperature.

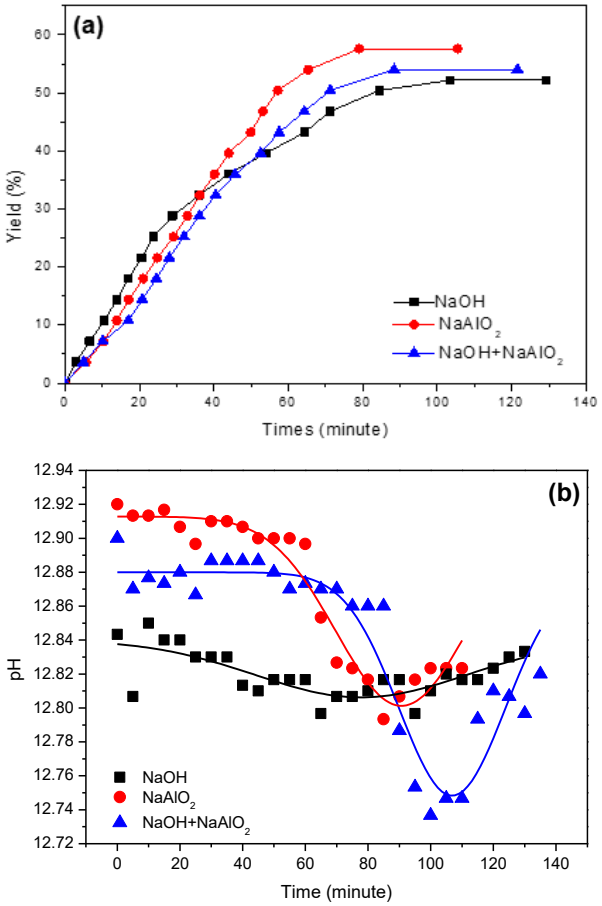

Figure 5. (a) The volume of hydrogen produced from different solutions (b) pH of solution over reaction time measured at room temperature.

Copyright © 2023, ISSN 1978-2993

from 293 K to 343 K. But this energy activation value is smaller compared to that of obtained for $NaAlO_2$ only, *i.e.*, 71 kJ.mol^{-1} as reported by Soler *et al.* [36] indicating the process still relies on NaOH.

Figure 5(a) shows the comparison of hydrogen yields among three different solutions, *i.e.* NaOH, $NaAlO_2$, and NaOH+$NaAlO_2$ for the same solution's pH of about 13. This indicates that the obtained yields and the reaction rate among these solutions are almost similar. To clarify the difference among the three solutions, a continuous pH measurement was undertaken during the hydrogen production. As seen in Figure 5(b), the pH remained stable in NaOH solution, indicating that the balance between OH^- consumption and re-emergence remained. The pH slightly decreased in $NaAlO_2$ and NaOH+$NaAlO_2$, suggesting that the consumption of OH^- ions was more than the re-emergence. It implies that during the decreasing pH reverse reaction (2) takes place surpressing the precipitation of $Al(OH)_3$. Once the accumulation of OH^- was high enough, the regeneration of NaOH and further continuous Al consumption occurred. Addition of NaOH in $NaAlO_2$ shows a pronounced surpressing $Al(OH)_3$ precipitation at the time longer than that of solely $NaAlO_2$ solution as expected from Cheng *et al.* [34].

3.2 Mechanism of Aluminum–Water Reaction with NaOH+$NaAlO_2$ Catalyst Support

The following process is based on the mechanism proposed by Yavor [43]. In the aluminum–water reaction, it is estimated that a hydration reaction occurs in three stages (Figure 6). In the initial stage, the hydration of the protective layer of Al_2O_3 from the surface of aluminum particles takes place. The non-porous Al_2O_3 layer on the surface is then replaced by a porous AlOOH layer. However, hydrogen formation is not yet maximized at this stage. Subsequently, in the rapid reaction stage, water penetrates the AlOOH layer and react with unreacted Al cores. Once the entire alumina layer is transformed into the AlOOH layer, the reaction rate is controlled by the thin new AlOOH film layer. Water diffuses through the holes on the surface of the AlOOH layer and react with Al cores, and this process continues until all the Al cores react with water. This process relies on the diffusion of water towards the Al cores, where the diffusion coefficient depends on activation energy and temperature.

The byproducts of the reaction determine the favorability of the reaction to occur. By adding a solution of $NaAlO_2$, various types of aluminates appear in the solution, including polymeric aluminate ions that act as nucleation centers for the formation of $Al(OH)_3$ crystals on the surface of aluminum [44]. The formation of the $Al(OH)_3$ layer on the aluminum surface captures water molecules, enabling the de-passivation effect of aluminates [36]. Thus, facilitating the reaction between aluminum and water to continue but at a lower rate. Aluminum hydroxides as byproducts are in the form of solid precipitates.

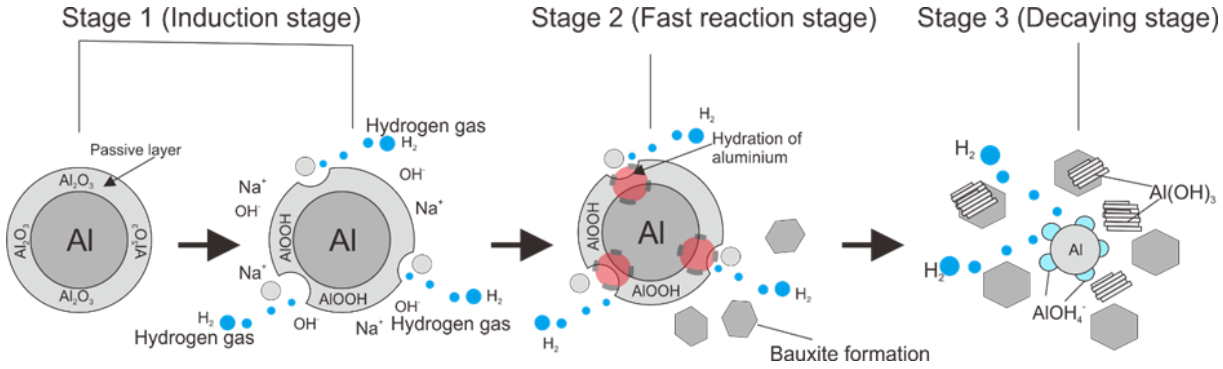

Figure 6. Mechanism of hydrogen formation from aluminum–water in the three phases of aluminum hydration kinetics.

Table 2. Average standard deviation (in mL) for the reaction kinetics model at different temperature.

Model	Temperature (°C)					
	32	40	50	60	70	80
Shrinking core model	5.5	5.8	6.8	3.9	4.1	4.4
Mass reduction model	15.7	10.0	26.7	26.4	31.7	32.9

Copyright © 2023, ISSN 1978-2993

3.3 Reaction Kinetics Modeling

The volume of hydrogen generated was evaluated by comparing the Mass Reduction Model (MRM) and the Shrinking Core Model (SCM) (Figure 7). It can be observed that the MRM is closer to the research results (Table 2). This is because the MRM observes the reduction in aluminum thickness over time. In the MRM, the thickness of the aluminum slab can be used to estimate the start and end times of the reaction, which can be observed on the thinnest side of the slab. In the kinetics of the reaction process, the thinnest side of the aluminum slab will degrade first, assuming that the hydration rate on each side is the same [39]. This process occurs gradually until the final stage, where the part of the slab that is nearly degraded will float and disappear from the edge towards the center of the aluminum slab.

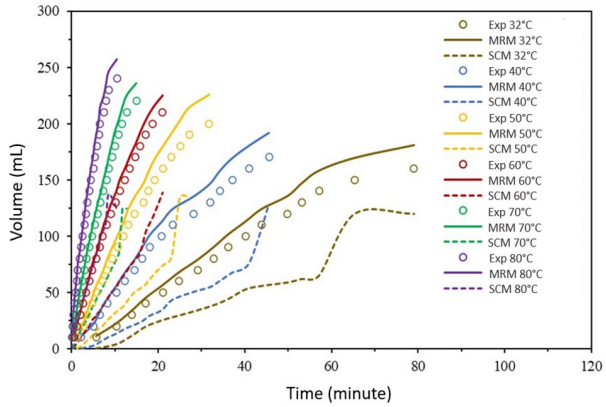

Figure 7. Comparison of the Mass Reduction Model (MRM) and the Shrinking Core Model (SCM) in reaction kinetics modeling.

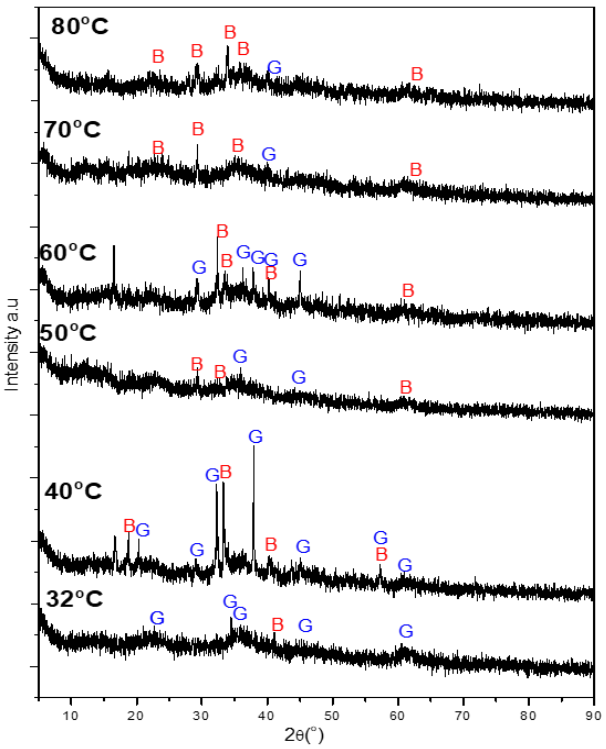

Figure 8. XRD patterns of aluminum can waste residues after reactions at various operating temperatures.

On the other hand, SCM refers to the three-phase approach controlled by thin-film diffusion, chemical reaction, and ash control diffusion [38]. The SCM is created by assuming that aluminum particles are spherical and remain in that form during the oxidation process. Additionally, the chemical reaction occurs at the interface between aluminum and reaction products, while the temperature in the reaction zone remains constant during oxidation. Another assumption is that the oxidation reaction consists of three stages, where the induction stage is the first stage, and the second and third stages involve relatively rapid oxidation with kinetic limitations and the rate of water diffusion through the thick layer of oxidation products. This model can describe the second and third stages of the reaction well, but the proposed approach to describe the induction stage is still not accurate because there is no significant change in aluminum particles during this stage, and the reaction rate is still low. Previous research has reported that SCM is more suitable for faster reactions, while mass reduction modeling is more suitable for slower reactions. The results obtained suggest that aluminum with thinner thickness can be approximated with the SCM, while aluminum with thicker thickness can be approximated with the mass reduction model [45].

3.4 Characterization of Aluminum

XRD patterns of the Al samples after reactions at various operating temperatures show peaks indicating the presence of $Al(OH)_3$ gibbsite and bayerite (Figure 8). In the aluminum can samples at temperatures of 40, 60, and 80 ^oC, dominant gibbsite and bayerite peaks were observed on the lattice planes (001), (110),

Table 3. Aluminum–water reaction residues from XRD characterization.

Temperature (°C)	Residues (%)	
	Gibbsite	Bayerite
30	99.5	0.05
40	86.2	13.8
50	75.4	24.6
60	90.7	9.3
70	57.2	42.8
80	0.7	99.3

Copyright © 2023, ISSN 1978-2993

(112), (31−1), (30−1), (31−1), and (−214). Peak validation displayed in the samples was performed using software with data from the *Crystallography Open Database* as a reference. The data were obtained using the COD ID 9008237 (gibbsite) and COD ID 9010964 (bayerite) approaches. Based on Figure 8 the reaction products consist of characteristic spectra of aluminum hydroxides (gibbsite and bayerite) with the highest percentage as listed in Table 3. No Al patterns were observed in the products, indicating that the reaction has been fully processed, and all the waste Al can samples have been converted into aluminum hydroxides. Therefore, it can be said that Al and water molecules as raw materials have reacted completely with the assistance of an alkaline solution as a catalyst.

According to Addai-Mensah *et al.* [46], gibbsite and bayerite always nucleate at temperatures below 65 °C from caustic aluminate solutions. Bayerite has a higher solubility than gibbsite [39] and when bayerite already coexists with gibbsite, it means that the actual solubility is significantly higher than gibbsite solubility used [47]. In Table 3, even though both gibbsite and bayerite coexist, up to 70 °C gibbsite remains predominant due to its tendency to nucleate profoundly [48], in addition, gibbsite is more stable than bayerite by about 8 kJ/mol [49]. At a temperature of 80 °C, the gibbsite becomes less since only crystal growth occurs, giving rise to the formation of a few aggregates of gibbsite. Following XRD results, Figure 9 shows the SEM images of the byproducts which indicate the typical morphology of gibbsite and bayerite being dominant at low temperature and high temperature, respectively.

Identification of Al−O and O−H functional groups formed from aluminum–water reaction residues using FTIR in the form of $(Al(OH)_3)$, bayerite, and gibbsite was shown in Figure 10. The FTIR spectra of gibbsite generally show absorption bands in the range of 3700–3200 cm^{-1}, while bayerite exhibits absorption bands

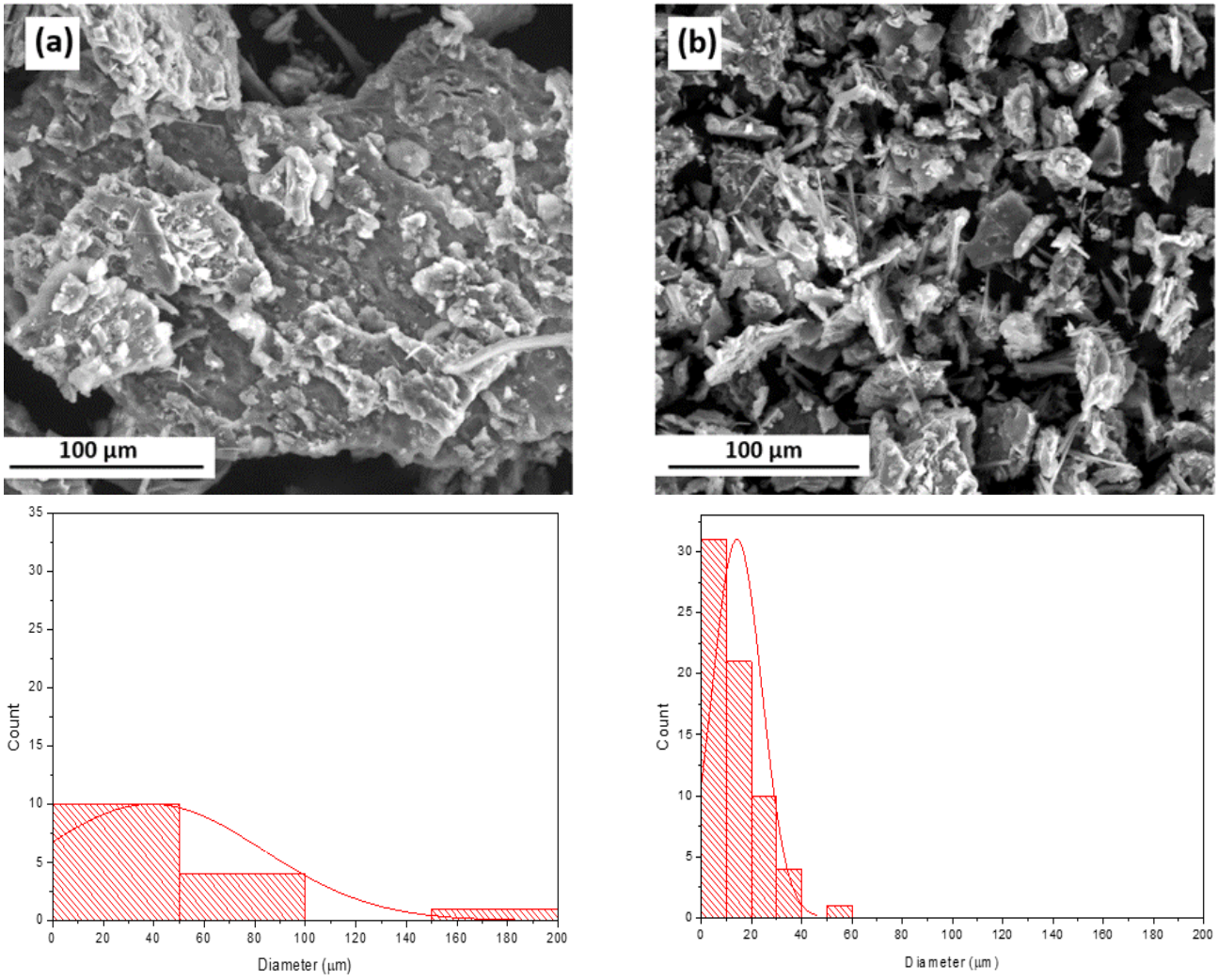

Figure 9. Morphology of reaction products at temperatures of (a) 32 °C and (b) 80 °C.

Copyright © 2023, ISSN 1978-2993

in the range of 3500–3100 cm^{-1}, which corresponds to the stretching vibrations of O–H bonds in hydroxyl groups of minerals. O–H (stretching) functional groups in the mixed phase (bayerite, gibbsite) were found at wavelengths of 3299, 3280, 3277, 3268, and 3265 cm^{-1}, representing extensions of AlO_4 as observed in a study by Prabu *et al.* [50].

Other broad absorption bands for gibbsite are observed in the range of 1650–1400 cm^{-1}, while bayerite is observed in the range of 1700–1400 cm^{-1}, distributed in the bending vibrations of O–H bonds. O–H (bending) functional groups in the mixed phase were found at wavelengths 1651, 1648, 1641, 1569, 1563, 1560, 1559, and 1555 cm^{-1}, corresponding to the vibrations of AlO_6. In the spectra of gibbsite and bayerite, there are weak absorption bands in the ranges of 800–400 cm^{-1}, 1000–600 cm^{-1}, and 1200–800 cm^{-1}, which are caused by Al–O bonds in minerals. Al–O functional groups in the mixed phase appear at wavelengths of 1179, 1157, 1155, 1153, 976, 973, 972, 966, 961, 847, 845, 844, 764, 757, 756, 667, 666, 660, and 658 cm^{-1}, corresponding to the vibrations of AlO_6. The broad (bending) O–H wavelengths indicate the presence of weaker hydrogen bonds, while the sharp (stretching) O–H wavenumbers indicate strong and concentrated hydrogen bonds [51]. From the residue spectrum, it can be analyzed that both bayerite and gibbsite structures are present, which is in accord with the XRD and SEM results.

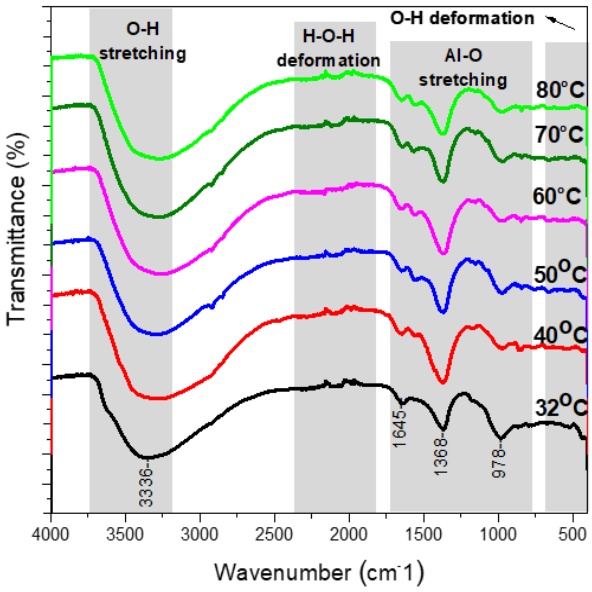

Figure 10. FTIR spectra of aluminum can waste residues after reactions at various studied temperatures.

4. Conclusions

In this work, the mixture between NaOH and $NaAlO_2$ catalysts was used to modify the water ionic species, and the modification mechanism was clarified. Hydrogen production from solution mixture has similar yields and rate compared to those of NaOH and $NaAlO_2$ solutions. However, the reverse reaction has occurred for both $NaAlO_2$ and mixture solutions causing $Al(OH)_3$ surpression. From the two studied models, the MRM fits the experiments with an average standard deviation of 5.1 mL, while the SCM tends to show underestimated values with an averaged standard deviation of 23.9 mL. It was found that both gibbsite and bayerite coexist at all temperatures studied in the byproducts and the phase transformation of transition of both phases strongly depends on the temperature, where gibbsite and bayerite become dominant at temperatures below 70 °C and 80 °C, respectively.

Acknowledgments

This work was supported by research grant No. 14433/UN25.3.1/LT/2022 (Penelitian MBKM) from Universitas Jember for M. Muharja, A.I. Khamil, and S.N. Fadilah. This research was also supported by research grant No. 659/PKS/ITS/2022 (Penelitian Kerjasama Antar Perguruan Tinggi) from Institut Teknologi Sepuluh Nopember for N. Fadhilah, D.D. Risanti, and R.A. Wahyuono.

CRediT Author Statement

The conception and design of the study were collaborative efforts involving all authors. Data running and analysis were performed by Nur Fadhilah and Siska Nuri Fadilah. The validation and visualization were executed by Achri Isnan Khamil and Dendy Satrio. Doty Dewi Risanti, Ruri Agung Wahyuono carried out review and editing. Nur Fadhilah wrote the original draft, managed this work. Maktum Muharja supervised the works carried out by Achri Isnan Khamil and Siska Nuri Fadhilah. All authors read and commented on previous versions of the manuscript and approved the final manuscript.

Copyright © 2023, ISSN 1978-2993

References

[1] Londono-Pulgarin, D., Cardona-Montoya, G., Restrepo, J.C., Munoz-Leiva, F. (2021). Fossil or bioenergy? Global fuel market trends. *Renewable and Sustainable Energy Reviews*, 143, 110905. DOI: 10.1016/j.rser.2021.110905.

[2] Oliveira, T.C.G., Hanlon, K.E., Interlandi, M.A., Torres-Mayanga, P.C., Silvello, M.A.C., Lachos-Perez, D., Timko, M.T., Rostagno, M.A., Goldbeck, R., Forster-Carneiro, T. (2020). Subcritical water hydrolysis pretreatment of sugarcane bagasse to produce second generation ethanol. *Journal of Supercritical Fluids*, 164, 104916. DOI: 10.1016/j.supflu.2020.104916.

[3] Irankhah, A., Seyed Fattahi, S.M., Salem, M. (2018). Hydrogen generation using activated aluminum/water reaction. *International Journal of Hydrogen Energy*, 43 (33), 15739–15748. DOI: 10.1016/j.ijhydene.2018.07.014.

[4] Holechek, J.L., Geli, H.M.E., Sawalhah, M.N., Valdez, R. (2022). A Global Assessment : Can Renewable Energy Replace Fossil Fuels by 2050?. *Sustainability*, 14(8), 4792. DOI: 10.3390/su14084792.

[5] Rin, T., Sangwichien, C., Yamsaengsung, R., Reungpeerakul, T. (2021). Hydrogen generation from the hydrolysis of aluminum promoted by Ni–Li–B catalyst. *International Journal of Hydrogen Energy*, 46 (56), 28450–28461. DOI: 10.1016/j.ijhydene.2021.06.101.

[6] Singh, K.K., Meshram, A., Gautam, D., Jain, A. (2019). Hydrogen production using waste aluminium dross: From industrial waste to next-generation fuel. *Agronomy Research*, 17, 1199–1206. DOI: 10.15159/AR.19.022

[7] Meshram, A., Jain, A., Rao, M.D., Singh, K.K. (2019). From industrial waste to valuable products: preparation of hydrogen gas and alumina from aluminium dross. *Journal of Material Cycles and Waste Management*, 21(4), 984–993. DOI: 10.1007/s10163-019-00856-y.

[8] Bolt, A., Dincer, I., Agelin-Chaab, M. (2020). Experimental study of hydrogen production process with aluminum and water. *International Journal of Hydrogen Energy*, 45 (28), 14232–14244. DOI: 10.1016/j.ijhydene.2020.03.160

[9] Dawood, F., Anda, M., Shafiullah, G.M. (2020). Hydrogen production for energy: An overview. *International Journal of Hydrogen Energy*, 45 (7), 3847–3869. DOI: 10.1016/j.ijhydene.2019.12.059.

[10] Osman, A.I., Mehta, N., Elgarahy, A.M., Hefny, M., Hinai, A. Al, Muhtaseb, H. Al, Rooney, D.W. (2022). Hydrogen production, storage, utilisation and environmental impacts : a review. *Environmental Chemistry Letters*, 20, 153–188. DOI: 10.1007/s10311-021-01322-8.

[11] Midilli, A., Kucuk, H., Topal, M.E., Akbulut, U., Dincer, I. (2021). A comprehensive review on hydrogen production from coal gasification: Challenges and Opportunities. *International Journal of Hydrogen Energy*, 46(50), 25385–25412. DOI: 10.1016/j.ijhydene.2021.05.088.

[12] Chen, J., Xu, W., Zhang, F., Zuo, H., E, J., Wei, K., Liao, G., Fan, Y. (2019). Thermodynamic and environmental analysis of integrated supercritical water gasification of coal for power and hydrogen production. *Energy Conversion and Management*, 198, 111927. DOI: 10.1016/j.enconman.2019.111927

[13] Chen, J., Wang, L., Cheng, Z., Lu, L., Guo, L., Jin, H., Zhang, D., Wang, R., Liu, S. (2021). Performance simulation and thermodynamics analysis of hydrogen production based on supercritical water gasification of coal. *International Journal of Hydrogen Energy*, 46 (56), 28474–28485. DOI: 10.1016/j.ijhydene.2021.06.097.

[14] Prasad, R. (2009). Design of a Simple and Cheap Water Electrolyser for the Production of Solar Hydrogen. *Bulletin of Chemical Reaction Engineering & Catalysis*, 4 (1), 10–15. DOI: 10.9767/bcrec.4.1.7113.10-15

[15] Burton, N.A., Padilla, R. V., Rose, A., Habibullah, H. (2021). Increasing the efficiency of hydrogen production from solar powered water electrolysis. *Renewable and Sustainable Energy Reviews*, 135, 110255. DOI: 10.1016/j.rser.2020.110255

[16] Shiva Kumar, S., Lim, H. (2022). An overview of water electrolysis technologies for green hydrogen production. *Energy Reports*, 8, 13793–13813. DOI: 10.1016/j.egyr.2022.10.127.

[17] Terlouw, T., Bauer, C., McKenna, R., Mazzotti, M. (2022). Large-scale hydrogen production via water electrolysis: a techno-economic and environmental assessment. *Energy and Environmental Science*, 15 (9), 3583–3602. DOI: 10.1039/d2ee01023b.

[18] Anzelmo, B., Wilcox, J., Liguori, S. (2018). Hydrogen production via natural gas steam reforming in a Pd-Au membrane reactor. Comparison between methane and natural gas steam reforming reactions. *Journal of Membrane Science*, 568, 113–120. DOI: 10.1016/j.memsci.2018.09.054

Copyright © 2023, ISSN 1978-2993

[19] El Hajj Chehade, A.M., Daher, E.A., Assaf, J.C., Riachi, B., Hamd, W. (2020). Simulation and optimization of hydrogen production by steam reforming of natural gas for refining and petrochemical demands in Lebanon. *International Journal of Hydrogen Energy*, 45 (58), 33235–33247. DOI: 10.1016/j.ijhydene.2020.09.077.

[20] Boretti, A., Banik, B.K. (2021). Advances in Hydrogen Production from Natural Gas Reforming. *Advanced Energy and Sustainability Research*, 2 (11), 2100097. DOI: 10.1002/aesr.202100097.

[21] Chibane, L. (2018). Simulation study of a membrane reactor for ultrapure hydrogen recovery from methanol steam reforming reaction under periodic steady-state. *Bulletin of Chemical Reaction Engineering & Catalysis*, 13 (2), 275–285. DOI: 10.9767/bcrec.13.2.1340.275-285

[22] Razak, S.A., Bahruji, H., Mahadi, A.H., Yun, H.W. (2022). H_2O_2 Exfoliation of TiO_2 for Enhanced Hydrogen Production from Photocatalytic Reforming of Methanol. *Bulletin of Chemical Reaction Engineering & Catalysis*, 17 (2), 420–429. DOI: 10.9767/BCREC.17.2.13920.420-429

[23] Lesmana, D., Wu, H.S. (2017). $Cu/ZnO/Al_2O_3/Cr_2O_3/CeO_2$ catalyst for hydrogen production by oxidative methanol reforming via washcoat catalyst preparation in microchannel reactor. *Bulletin of Chemical Reaction Engineering & Catalysis*, 12(3), 384–392. DOI: 10.9767/bcrec.12.3.966.384-392

[24] Singla, S., Sharma, S., Basu, S., Shetti, N.P., Aminabhavi, T.M. (2021). Photocatalytic water splitting hydrogen production via environmental benign carbon based nanomaterials. *International Journal of Hydrogen Energy*, 46 (68), 33696–33717. DOI: 10.1016/j.ijhydene.2021.07.187.

[25] Siavash Moakhar, R., Hosseini-Hosseinabad, S.M., Masudy-Panah, S., Seza, A., Jalali, M., Fallah-Arani, H., Dabir, F., Gholipour, S., Abdi, Y., Bagheri-Hariri, M., Riahi-Noori, N., Lim, Y.F., Hagfeldt, A., Saliba, M. (2021). Photoelectrochemical Water-Splitting Using CuO-Based Electrodes for Hydrogen Production: A Review. *Advanced Materials*, 33(33) DOI: 10.1002/adma.202007285

[26] Chen, Z., Wei, W., Ni, B.J. (2021). Cost-effective catalysts for renewable hydrogen production via electrochemical water splitting: Recent advances. *Current Opinion in Green and Sustainable Chemistry*, 27, 100398. DOI: 10.1016/j.cogsc.2020.100398.

[27] Acar, C., Dincer, I. (2019). Review and evaluation of hydrogen production options for better environment. *Journal of Cleaner Production*, 218, 835–849. DOI: 10.1016/j.jclepro.2019.02.046

[28] Bolt, A., Dincer, I., Agelin-Chaab, M. (2021). A Review of Unique Aluminum-Water Based Hydrogen Production Options. *Energy and Fuels*, 35 (2), 1024–1040. DOI: 10.1021/acs.energyfuels.0c03674

[29] Buryakovskaya, O.A., Vlaskin, M.S., Ryzhkova, S.S. (2019). Hydrogen production properties of magnesium and magnesium-based materials at low temperatures in reaction with aqueous solutions. *Journal of Alloys and Compounds*, 785, 136–145. DOI: 10.1016/j.jallcom.2019.01.003.

[30] Desai, M.A., Vyas, A.N., Saratale, G.D., Sartale, S.D. (2019). Zinc oxide superstructures: Recent synthesis approaches and application for hydrogen production via photoelectrochemical water splitting. *International Journal of Hydrogen Energy*, 2091–2127. DOI: 10.1016/j.ijhydene.2018.08.042.

[31] Trowell, K., Goroshin, S., Frost, D., Bergthorson, J. (2022). Hydrogen production rates of aluminum reacting with varying densities of supercritical water. *RSC Advan*ces, 12(20), 12335–12343. DOI: 10.1039/d2ra01231f.

[32] Setiani, P., Watanabe, N., Sondari, R.R., Tsuchiya, N. (2018). Mechanisms and kinetic model of hydrogen production in the hydrothermal treatment of waste aluminum. *Materials for Renewable and Sustainable Energy*, 7(2), 1–13. DOI: 10.1007/s40243-018-0118-8.

[33] Wysocka, J., Cieslik, M., Krakowiak, S., Ryl, J. (2018). Carboxylic acids as efficient corrosion inhibitors of aluminium alloys in alkaline media. *Electrochimica Acta*, 289, 175–192. DOI: 10.1016/j.electacta.2018.08.070.

[34] Cheng, Y. Lin, Xie, H. Jun, Cao, J. Hui, Cheng, Y. liang (2021). Effect of NaOH on plasma electrolytic oxidation of A356 aluminium alloy in moderately concentrated aluminate electrolyte. *Transactions of Nonferrous Metals Society of China (English Edition)*, 31(12), 3677–3690. DOI: 10.1016/S1003-6326(21)65756-4.

[35] Ilyin, A.P., Mostovshchikov, A. V., Nazarenko, O.B., Zmanovskiy, S. V. (2019). Heat release in chemical reaction between micron aluminum powders and water. *International Journal of Hydrogen Energy*, 44(52), 28096–28103. DOI: 10.1016/j.ijhydene.2019.09.072.

[36] Soler, L., Candela, A.M., Macanás, J., Muñoz, M., Casado, J. (2009). In situ generation of hydrogen from water by aluminum corrosion in solutions of sodium aluminate. *Journal of Power Sources*, 192 (1), 21–26. DOI: 10.1016/j.jpowsour.2008.11.009.

Copyright © 2023, ISSN 1978-2993

[37] Jansson, R.E.W. (1980). *Electrochemical Reaction Engineering*.

[38] Wang, X., Li, G., Eckhoff, R.K. (2021). Kinetics study of hydration reaction between aluminum powder and water based on an improved multi-stage shrinking core model. *International Journal of Hydrogen Energy*, 46(67), 33635–33655. DOI: 10.1016/j.ijhydene.2021.07.191.

[39] Salueña-Berna, X., Marín-Genescà, M., Vidal, L.M., Dagà-Monmany, J.M. (2021). Waste aluminum application as energy valorization for hydrogen fuel cells for mobile low power machines applications. *Materials*, 14(23) DOI: 10.3390/ma14237323.

[40] Kasantikul, B., Poomsawat, W. (2020). Hydrogen Production from Aluminium-Water Reactions: Thermodynamic Properties Analysis. 13(3), 1–13.

[41] Kandasamy, J., Mutlu, R.N., Eroğlu, E., Karaca, M., Toffoli, H., Gökalp, İ. (2023). Hydrogen production using aluminum-water splitting: A combined experimental and theoretical approach. *International Journal of Hydrogen Energy*. DOI: 10.1016/j.ijhydene.2023.04.068

[42] Zhuk, A.Z., Sheindlin, A.E., Kleymenov, B. V., Shkolnikov, E.I., Lopatin, M.Y. (2006). Use of low-cost aluminum in electric energy production. *Journal of Power Sources*, 157(2), 921–926. DOI: 10.1016/j.jpowsour.2005.11.097.

[43] Yavor, Y. (2016). Aluminum-water reaction mechanism – modeling of the different reaction stages. *14th Int Energy Convers Eng Conf 2016*. DOI: 10.2514/6.2016-5021

[44] Li, J., Yin, Z., Ding, Z., Liu, W., Wei, T., Chen, Q., Zhang, W. (2016). Homogeneous nucleation of $Al(OH)_3$ crystals from supersaturated sodium aluminate solution investigated by in situ conductivity. *Hydrometallurgy*, 163, 77–82. DOI: 10.1016/j.hydromet.2016.03.010.

[45] Maulana, F.R., Fadhilah, N., Agung Wahyuono, R., Risanti, D.D. (2023). Hydrogen Production from Waste Aluminum Foil AA1235 Using the Aluminum-Water Reaction Method with Thickness Variations. *Advanced Materials Research*, 1175, 9–15. DOI: 10.4028/p-587vv6.

[46] Addai-Mensah, J., Gerson, A.R., Prestidge, C.A., Ametov, I., Ralston, J. (1998). Interaction between Gibbsite Crystals in Supersaturated Caustic Aluminate Solutions. *Light MetaIs*, 159–166.

[47] Rusanen, M., Koponen, I.T., Ala-Nissila, T. (2002). Meandering instability of curved step edges on growth of a crystalline cone. *Surface Science*, 507–510, 305–310. DOI: 10.1016/S0039-6028(02)01262-1.

[48] Misra, C. (2003). Aluminum Oxide (Hydrated). *Kirk Othmer Encyclopdia of Chemical Technology*, 2, 421–433.

[49] Demichelis, R., Civalleri, B., Noel, Y., Meyer, A., Dovesi, R. (2008). Structure and stability of aluminium trihydroxides bayerite and gibbsite: A quantum mechanical ab initio study with the Crystal06 code. *Chemical Physics Letters*, 465(4), 220–225. DOI: 10.1016/j.cplett.2008.09.070.

[50] Prabu, S., Wang, H.W. (2021). Hydrogen generation from the reaction of Al and H_2O using a synthesized $Al(OH)_3$ nanoparticle catalyst: The role of urea. *Catalysis Science and Technology*, 11(13), 4636–4649. DOI: 10.1039/d1cy00534k.

[51] Prabu, S., Wang, H.W. (2021). Improved hydrogen generation from Al/water reaction using different synthesized $Al(OH)_3$ catalyst crystalline phases. *International Journal of Energy Research*, 45(6), 9518–9529. DOI: 10.1002/er.6478

Copyright © 2023, ISSN 1978-2993